An ESR and ENDOR study of the Ag^0 center in KCl and NaCl†

G. E. Holmberg,*‡ W. P. Unruh, and R. J. Friauf
University of Kansas, Lawrence, Kansas 66044
(Received 3 February 1975)

Previous workers have determined that the Ag^0 center produced in alkali halides doped with silver and γ or x irradiated at 77 K is a silver atom in a substitutional cation site. Through the use of electron-nuclear double resonance (ENDOR) we have measured the hyperfine parameters of the first four neighbor shells about this Ag^0 center at 4 K in KCl and NaCl. Contrary to a suggestion made in an earlier study, no indication was found of a lattice vacancy near the Ag^0 center. For both crystals there was an anomalously high contact interaction with shell-4 nuclei. Quadrupole-interaction constants were in most cases quite different from those expected through consideration only of the effect of the extra electron at the silver lattice site. This difference probably is an indication of lattice distortion about the Ag^0 center. Extra structure which appeared in first-shell ENDOR spectra in both crystals was successfully accounted for as second-order hyperfine structure. Fabrication of the superhyperfine structure of the high-field ESR line from ENDOR parameters yielded good agreement for KCl but showed that not all of the ESR line broadening could be accounted for by interactions with the first four shells for the Ag^0 center in NaCl.

I. INTRODUCTION

The Ag^0 center in KCl was first identified in an ESR and optical study of γ- and x-irradiated KCl:^{109}Ag crystals by Delbecq *et al.*[1] Their model for the center was a silver atom in a substitutional cation site. The ESR spectrum of the Ag^0 center in KCl was successfully explained by a 649-G Fermi contact interaction between the silver electron in a $^2S_{1/2}$ ground state and its own spin-$\frac{1}{2}$ nucleus, along with superhyperfine (shf) interactions with six nearest-neighbor chlorine nuclei which give structure to each of the two ESR lines.

Seidel[2] performed electron-nuclear double-resonance (ENDOR) measurements on the Ag^0 center in KCl:Ag and verified the substitutional model. He identified ENDOR lines from neighbor shells 1, 3, and 4, but quoted no quadrupole interaction constant for shell 4. He was not able to identify a number of lines, some strongly anisotropic, in the frequency region between 0.9 and 2.2 MHz. He pointed out that these lines might indicate a lattice distortion which was possibly caused by a third-shell vacancy. An alternative explanation for these unidentified lines is proposed in the present investigation.

The study of the Ag^0 center using ESR was extended to other alkali chlorides by Baranov *et al.*[3-5] and to other potassium halides by Melnikov *et al.*[6] In the case of NaCl the shf structure of the two Ag^0 ESR lines was barely resolved in contrast to well-resolved shf structure for the Ag^0 center in KCl and LiCl. Baranov *et al.*[3] believed that the lack of resolution in the NaCl case could be due to the combined effects of a large Fermi contact interaction with shell-4 sodium nuclei and the larger magnetic moment of the ^{23}Na nucleus relative to the ^{39}K nucleus. This speculation is confirmed in the current investigation.

In the present study, ESR and ENDOR measurements were performed on γ-irradiated KCl:^{107}Ag and NaCl:^{107}Ag crystals at reduced temperatures. A single isotope of silver was used to simplify data interpretation. ENDOR lines from the first four shells of both cases were fit to a computer-diagonalized spin Hamiltonian. For each crystal the ENDOR parameters were used to generate a theoretical ESR shf structure and an envelope function for the 5*s* electron, and also used to infer probable distortions of the lattice. Second-order hyperfine structure was observed for some ENDOR lines and interpreted through the use of a two-neighbor spin Hamiltonian.

II. PROCEDURES

A. Experimental technique

Single crystals of KCl:^{107}Ag and NaCl:^{107}Ag were grown from reagent grade materials using the Kyropoulous technique. The KCl and NaCl melts contained 0.5 and 0.8 molar %, respectively, of ^{107}AgCl. The dopant was derived from metallic silver enriched to contain 98.54% ^{107}Ag.

Each sample was attached to the bottom of a TE_{102} *X*-band microwave cavity bottom, straddling a slot used for introduction of rf during ENDOR measurements. The cavity bottom with sample in place, was exposed to several Mrad of ^{60}Co γ radiation while at 77 K and thereafter was stored under liquid nitrogen. Prior to a spin resonance measurement, the cavity was attached to the end of an ESR-ENDOR probe taking care to minimize sample warming.

The ESR-ENDOR probe was connected to a superheterodyne ENDOR spectrometer similar to

that described by Unruh *et al.*[7] ESR measurements were performed in the standard manner at temperatures near 77 and 4 K. ENDOR measurements were performed near 4 K, with the ESR line partially saturated, by sweeping the rf up and down in frequency, and signal averaging the spectrometer output to enhance the signal to noise ratio. Comparison of the swept rf method with conventional method, in which the rf power is amplitude modulated and the ENDOR signal is detected with a lock-in amplifier, showed no detectable difference in position of the ENDOR peaks. The transient method was used because data could be gathered many times faster than was possible using the chopped technique.

B. ESR analysis

The ESR measurements were analyzed using a spin Hamiltonian containing Zeeman interactions and a Fermi contact interaction between the silver 5*s* electron and its own spin-$\frac{1}{2}$ nucleus

$$\mathcal{H} = g_e \mu_B \vec{H}\cdot\vec{S} + A^S \vec{I}^S\cdot\vec{S} - g_N^S \mu_N \vec{H}\cdot\vec{I}^S , \qquad (1)$$

where g_e and g_N^S are the g factors for the silver electron and silver nucleus, μ_B and μ_N are the Bohr and nuclear magnetons, S and I^S are the spin operators for the silver electron and silver nucleus, and H is the magnetic field. Equation (1) is the basis for the Breit-Rabi formula,[8] which was was used to compute A^S and g_e from the center positions of the two hyperfine lines.

C. ENDOR analysis

For determination of ENDOR parameters, the ENDOR spectra of this work are fitted to a spin Hamiltonian which includes hyperfine interactions between the silver 5*s* electron and its own nucleus and one neighbor nucleus, as well as Zeeman interactions of the electron and the two nuclei, and a quadrupole interaction between the neighbor nucleus and the electric field gradient at the neighbor site.

$$\mathcal{H} = g_e \mu_B \vec{H}\cdot\vec{S} + A^S \vec{I}^S\cdot\vec{S} - g_N^S \mu_N \vec{H}\cdot\vec{I}^S + A^\alpha \vec{I}^\alpha\cdot\vec{S} + \vec{I}^\alpha\cdot\vec{B}^\alpha\cdot\vec{S} + \vec{I}^\alpha\cdot\vec{Q}^\alpha\cdot\vec{I}^\alpha - g_N^\alpha \mu_N \vec{H}\cdot\vec{I}^\alpha , \qquad (2)$$

where

$$\vec{B}^\alpha = \begin{bmatrix} -b_1^\alpha & 0 & 0 \\ 0 & -b_2^\alpha & 0 \\ 0 & 0 & b_1^\alpha + b_2^\alpha \end{bmatrix},$$

$$\vec{Q}^\alpha = \frac{q^\alpha}{3} \begin{bmatrix} \eta^\alpha - 1 & & 0 \\ 0 & -\eta^\alpha - 1 & 0 \\ 0 & 0 & 2 \end{bmatrix},$$

$$q^\alpha = \frac{3eQ^\alpha}{4I^\alpha(2I^\alpha - 1)} \frac{\partial^2 V^\alpha}{\partial z^2} ,$$

$$\eta^\alpha = \left(\frac{\partial^2 V^\alpha}{\partial x^2} - \frac{\partial^2 V^\alpha}{\partial y^2}\right)\left(\frac{\partial^2 V^\alpha}{\partial z^2}\right)^{-1} .$$

The superscript α refers to neighbor nucleus α. A is the isotropic hyperfine interaction, $\vec{B}$ is the dipole-dipole interaction tensor, and $\vec{Q}$ is the quadrupole interaction tensor. We shall refer to b_1 and b_2 as dipole-dipole interaction constants, q as the quadrupole interaction constant, and η as the quadrupole asymmetry parameter. For axial symmetry, $b_1 = b_2 = b$ and $\eta = 0$. Q^α is the quadrupole moment for nucleus α, and V^α is the electric potential at nucleus α.

Since the neighbor nuclear spin is $\frac{3}{2}$ for all Na^+, K^+, or Cl^- neighbors, the spin Hamiltonian matrix has a dimensionality of 16. The matrix is computed and diagonalized by computer. The spin Hamiltonian parameters are adjusted to fit selected ENDOR lines from neighbors with the magnetic field oriented at 0° and 90° with respect to the line from neighbor to silver nucleus, since frequencies from these lines are most free from sample misorientation errors.

To first order the ENDOR frequencies ν_{ENDOR} for a neighbor α at a site of axial symmetry are given by

$$\nu_{\mathrm{ENDOR}} = \left| \pm (1/2h)\left[A^\alpha + b^\alpha(3\cos^2\theta^\alpha - 1)\right] + (q^\alpha/h)(M_I^\alpha - \tfrac{1}{2})(3\cos^2\theta^\alpha - 1) - \nu_K^\alpha \right| , \qquad (3)$$

where the plus and minus signs relate to the sign of the electron spin projection, h is Planck's constant, M_I^α is the spin projection of the neighbor nucleus final state, θ^α is the angle between the magnetic field and a line from neighbor nucleus to the silver nucleus, and $\nu_K^\alpha = g_N^\alpha \mu_N H/h$ is the nuclear-magnetic-resonance (NMR) frequency for nucleus α.

The presence of $S_+ I_-^S$ and $S_- I_+^S$ off-diagonal elements in the Fermi contact interaction between the silver electron and the silver nucleus in Eqs. (1) and (2) causes wave-function mixing between states with antiparallel electron and silver nuclear spins. This leads to second-order frequency shifts of approximately 10% in ENDOR transitions originating from mixed states which enable determination of the relative sign of the silver and chlorine nuclear g values.[2,9] The relative sign is determined to be negative as expected.[10]

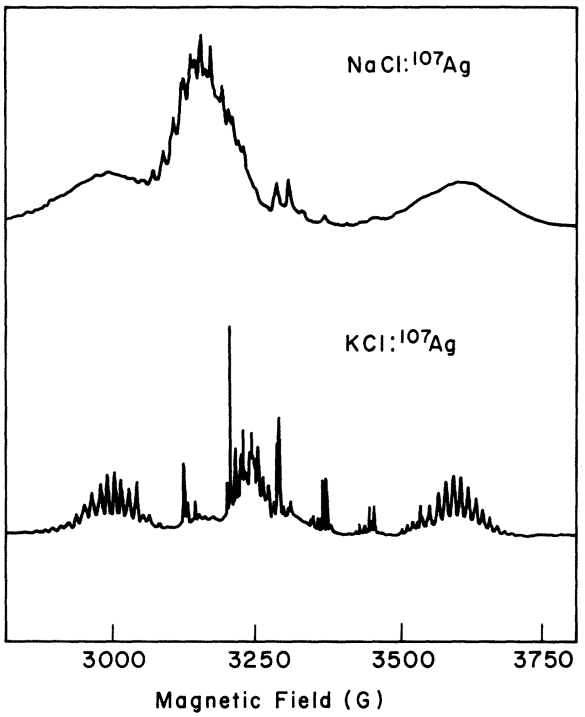

FIG. 1. ESR absorption spectra for γ-irradiated NaCl:^{107}Ag and KCl:^{107}Ag near 4 K for $\vec{H} \| [111]$. Cavity frequency, 9.29 GHz.

III. EXPERIMENTAL RESULTS

A. ESR

The ESR absorption spectra at 4 K for γ-irradiated NaCl:^{107}Ag and KCl:^{107}Ag single crystals are shown in Fig. 1 for H along [111]. The lines in the spectra at about 3000 and 3600 G are due to the Ag^0 center. The broad lines near 3250 G are believed to be associated with the Ag^{2+} center. The other sharp lines in the KCl spectrum are presumably caused by V_K centers, even though this sample had been warmed to about 225 K in order to decrease the V_K center contribution.

The spin Hamiltonian parameters from the Breit-Rabi formula are shown in Table I, along with comparative values measured by other workers. Since the other workers measured A^S for ^{109}Ag, their quoted values have been multiplied by $A^S(^{107}\text{Ag})/A^S(^{109}\text{Ag}) = 1712.56/1976.94$, the Fermi contact interaction ratios for the free silver atom measured by Wessel and Lew,[11] before inclusion in the table. The value of A^S attributed to Seidel was interpolated from a graph in his paper.[2]

Each of the ESR lines possesses shf structure due to interactions with neighboring nuclei. The largest interactions are with the six-nearest-neighbor chlorine ions in (1, 0, 0) positions, all of which are equivalent when the magnetic field is in the [111] direction. Since the chlorine nuclei have $I = \frac{3}{2}$, there should be 19 shf lines for this case (neglecting chlorine isotope effects). Interactions between the silver 5s electron and other neighbor shells will cause broadening of the shf lines. For the Ag^0 center in KCl, the shell-1 shf structure is resolved. But in the case of the Ag^0 center in NaCl, the shf structure is only barely resolved, even for a first derivative ESR spectrum (see Fig. 8).

B. ENDOR for Ag^0 center in KCl

The shell-1 lines occur between about 12 and 25 MHz and exhibit some interesting features. For each neighbor site, lines are observed at about

TABLE I. Electron g values and Fermi contact interactions for the Ag^0 center in KCl:^{107}Ag and NaCl:^{107}Ag. Since A^S was measured by other workers for ^{109}Ag, the values listed have been altered by the ratio $A^S(^{107}\text{Ag})/A^S(^{109}\text{Ag})$ for the free atom.[e] Seidel's value was interpolated from a graph.

		Present work		Other workers	
Crystal	Temperature (K)	g_e	A^S (G)	g_e	A^S (G)
KCl:^{107}Ag	77	1.9963 ± 0.0005	584 ± 1.5	2.000 ± 0.003 [a]	562 ± 2 [a]
					590 [b]
	4	1.9964 ± 0.0005	590 ± 1.5	1.995 ± 0.005 [c]	589.5 ± 2 [c]
NaCl:^{107}Ag	77	1.9951 ± 0.0014	582 ± 3.5	1.999 ± 0.003 [d]	579 ± 2.5 [d]
	4	1.9951 ± 0.0005	583 ± 1.5		

[a] C. J. Delbecq, W. Hayes, M. C. M. O'Brien, and P. W. Yuster, Proc. R. Soc. A 271, 243 (1963).

[b] H. Seidel, Phys. Lett. 6, 150 (1963).

[c] N. I. Melnikov, R. A. Zhitnikov, and P. G. Baranov, Fiz. Tverd. Tela 13, 1337 (1971) [Sov. Phys.-Solid State 13, 1117 (1971)].

[d] P. G. Baranov, R. A. Zhitnikov, and N. I. Melnikov, Phys. Status Solidi 30, 851 (1968).

[e] G. Wessel and H. Lew, Phys. Rev. 92, 641 (1953).

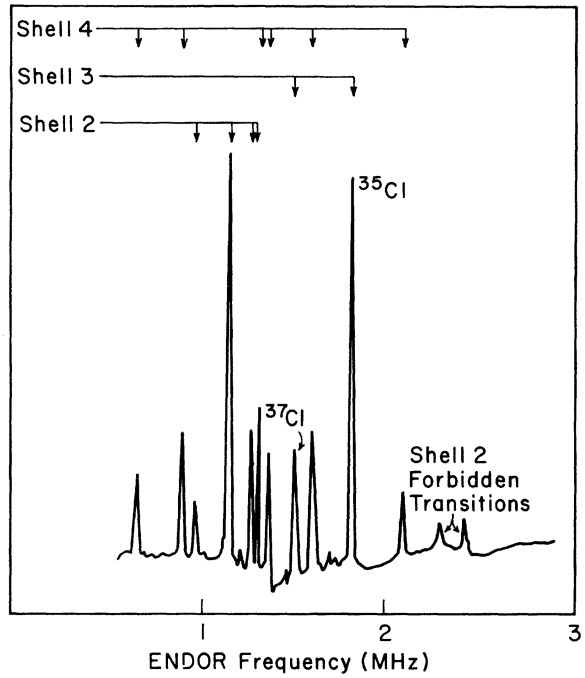

FIG. 2. ENDOR spectrum of shells 2–4 for the Ag^0 center in KCl:^{107}Ag. $H = 3616 \pm 1$ G and parallel to [100].

half the hyperfine interaction frequency plus and minus the NMR frequency for the chlorine isotope in question. The lines observed at plus the NMR frequency, those originating from transitions among ground-state energy levels [see Eq. (3)], are much more intense than those observed at minus the NMR frequency. The intensity difference is probably caused by differing relaxation paths for the higher and lower Zeeman-split sets of Ag^0 center energy levels. The other interesting feature present is second-order hyperfine structure, which causes ^{35}Cl lines to have a complicated structure. Discussion of second-order hyperfine structure will be delayed until Sec. IIID. From second-order frequency shifts, the quadrupole interaction constant was determined to be positive with respect to the nuclear g value for chlorine.[12]

The overall ENDOR spectrum for shells 2–4 is shown in Fig. 2. All lines that are observed are identified. Only the highest-frequency ENDOR lines, those from transitions among ground-state levels, are seen for these shells, and consequently the sign of the quadrupole constant cannot be determined for these shells. Forbidden ENDOR transitions which involve $\Delta M_I = \pm 2$ for shells-2 and -4 nuclei, and $\Delta M_I = \pm 3$ for shell-4 nuclei are observed for some magnetic field orientations. These forbidden transitions are caused by relatively large shell-2 and shell-4 quadrupole interaction constants, together with the large asymmetry parameter in the case of shell 2.

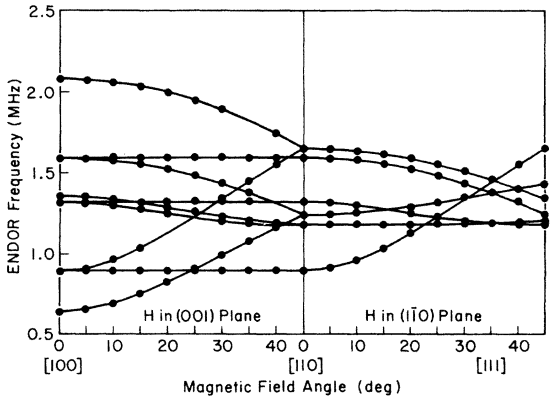

FIG. 3. ENDOR angular dependence of shell-4 ^{39}K neighbors for the Ag^0 center in KCl:^{107}Ag. $H = 3616 \pm 1$ G in the (001) plane; $H = 3621 \pm 1$ G in the (1$\bar{1}$0) plane. For this figure and subsequent angular dependence figures, solid circles represent experimental points; angular uncertainties are less than $\pm 1°$; frequency uncertainties, when not shown, are smaller than the symbol; and solid lines represent the theoretical angular behavior of the ENDOR lines, computed from the ESR and ENDOR parameters in Tables I–III.

The ENDOR lines from shell 3 occur between 1.7 and 2.0 MHz and present no interpretation difficulties.

The angular behavior of shell-4 ENDOR lines for magnetic field rotation in (001) and (1$\bar{1}$0) planes is shown in Fig. 3. For the magnetic field along [100] the separation of the outer lines represents four times the quadrupole interaction constant. Because of the relatively large quadrupole interaction constant, off-diagonal quadrupole matrix elements have a sizeable effect if the magnetic field is not along the line connecting the neighbor and silver nuclei. Hence, it is necessary in this case to do a com-

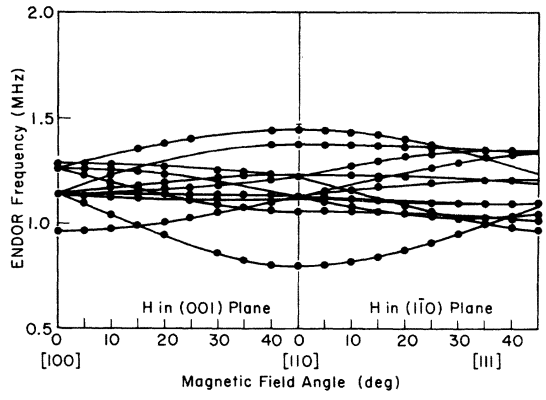

FIG. 4. ENDOR angular dependence of shell-2 ^{39}K neighbors for the Ag^0 center in KCl:^{107}Ag. $H = 3616 \pm 1$ G in the (001) plane; $H = 3621 \pm 1$ G in the (1$\bar{1}$0) plane.

puter diagonalization of the spin Hamiltonian so that higher-order terms from off-diagonal elements can be taken into account.

Figure 4 gives the angular dependence of the shell-2 ENDOR spectrum. Some experimental points are missing because of overlap with shell-4 lines. Shell-2 sites possess C_{2v} symmetry, which is not sufficient to force axial symmetry. However, the twofold axis and the two reflection planes of C_{2v} symmetry do fix the principal axes for tensor interactions along the x, y, and z axes shown in Fig. 5. The two outer lines in Fig. 4 for the magnetic field along a [100] direction are the outer quadrupole-split lines for the magnetic field along an x axis. The two outer lines for the magnetic field along [110] are the outer quadrupole-split lines when the magnetic field is along a y axis. The difference in splitting in these two situations is indicative of a sizeable quadrupole asymmetry parameter for this case.

As with the shell-4 spectrum, computer diagonalization is essential to the identification of shell 2. For the magnetic field along [100] lines are expected from two groups of shell-2 neighbors. One group of 4 neighbors sees the magnetic field as pointing in the direction of a shell-3 neighbor. This group gives three about equally split lines. The other group, comprised of eight neighbors which see the magnetic field at 45° in the $y-z$ plane, also gives rise to three ENDOR lines. However, off-diagonal elements cause two of these lines virtually to coincide in frequency, a feature which made initial identification difficult.

The spin Hamiltonian parameters used to fit the first four shells for the Ag^0 center in KCl are shown in Table II, together with parameters reported by Seidel. There is close agreement with the Seidel values with the exception of shell 4. The disagreement in that case is probably because Seidel did not include the quadrupole interaction

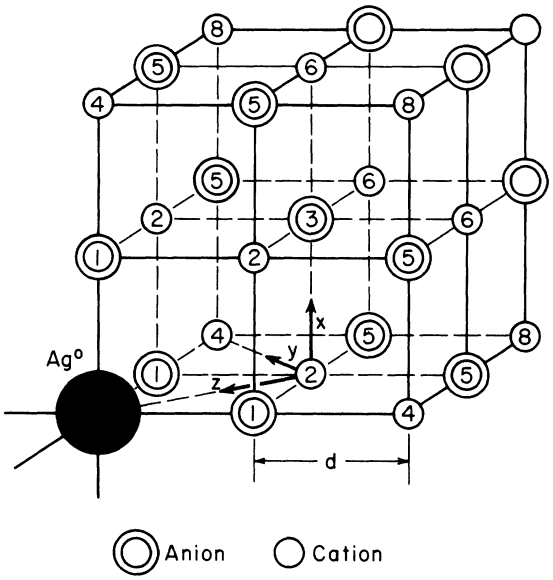

FIG. 5. Ag^0 center model. The shell numbers are indicated for shells 1–8. The principal axes x, y, and z of the anisotropic hyperfine and quadrupole tensors are shown for shell 2.

constant for shell 4. All observed ENDOR lines are accounted for and there is no indication of a lattice vacancy near the Ag^0 center.

C. ENDOR for Ag^0 center in NaCl

The spectrum is analogous to that observed in KCl, but the lines for the first four shells appear in separate groups. The first shell lines occur between about 25 and 42 MHz. The lines for ENDOR transitions from upper Zeeman states are even less intense than for the KCl case. Second-order hyperfine structure, which will be discussed in detail later, is more apparent than in KCl because of the larger hyperfine-structure param-

TABLE II. Spin Hamiltonian parameters for the Ag^0 center in KCl. The values in parentheses were determined by Seidel. [a]

Shell	Nucleus	A/h (MHz)	b/h (MHz)	q/h (MHz)
1	^{35}Cl	37.86 ± 0.10 (38.2)	3.91 ± 0.06 (3.85)	+0.39 ± 0.04 (0.40)
2	^{39}K	0.886 ± 0.007	$b_1/h = 0.059 \pm 0.011$ $b_2/h = 0.068 \pm 0.016$	$q/h = 0.081 \pm 0.004$ $\eta = 3.03 \pm 0.12$
3	^{35}Cl	0.599 ± 0.010 (0.590)	0.083 ± 0.006 (0.082)	0.012 ± 0.005 (0.012)
4	^{39}K	1.144 ± 0.013 (0.95)	0.079 ± 0.006 (0.105)	0.358 ± 0.005

[a] H. Seidel, Phys. Lett. 6, 150 (1963).

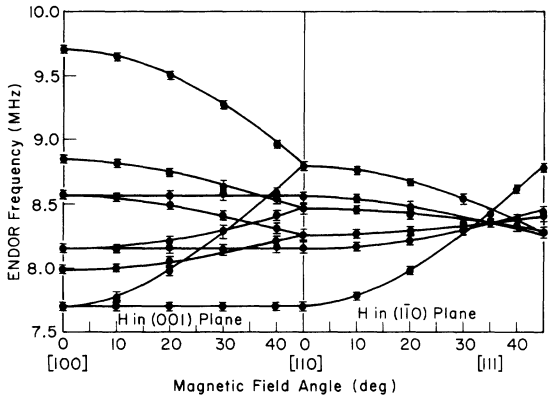

FIG. 6. ENDOR angular dependence of shell-4 ^{23}Na neighbors for the Ag^0 center in NaCl:^{107}Ag. $H = 3602 \pm 1$ G in both the (001) and (1$\bar{1}$0) planes.

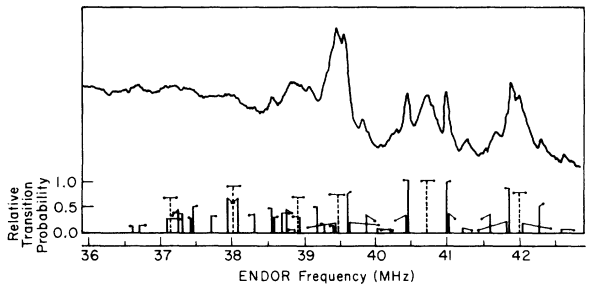

FIG. 7. Experimental and theoretical ENDOR spectra of shell-1 ^{35}Cl neighbors for the Ag^0 center in NaCl:^{107}Ag for $\vec{H} \parallel [100]$. The vertical dashed lines represent the relative ENDOR transition probabilities for the ^{35}Cl neighbor in ^{35}Cl-^{37}Cl pair. The vertical solid lines represent the relative ENDOR transition probabilities for a ^{35}Cl-^{35}Cl pair. The dots represent new theoretical line positions when A^α is shifted by ± 0.2 MHz or b^α is shifted by ± 0.1 MHz, with the average of A^α or b^α held constant to the best-fit values.

eters in the NaCl case. Second-order frequency shifts indicate a positive quadrupole interaction constant for shell 1. Shell-3 lines occur between 2.0 and 2.9 MHz. The interpretation of these lines presents no difficulty.

The shell-4 ^{23}Na ENDOR lines are located between 7.5 and 10 MHz. ^{23}Na has 100% natural abundance and a nuclear spin of $\frac{3}{2}$. The angular dependence of the shell-4 spectrum is shown in Fig. 6. As is true for KCl, the set of ENDOR lines at half the hyperfine interaction frequency minus the neighbor NMR frequency is not observed for shells 2–4.

The ENDOR parameters for the first four shells for the Ag^0 center in NaCl are summarized in Table III. From ESR data, Baranov *et al.*,[3] measured the Ag^0 center Fermi contact and dipole-dipole interaction constants for interactions with shell-1 ^{35}Cl nuclei in NaCl to be 68.3 and 5.6 MHz, respectively, close to our ENDOR values. As the discussion will illustrate, the general behavior is remarkably similar for the Ag^0 centers in the two crystals.

D. Second-order hyperfine structure

The ENDOR spectrum for first-shell ^{35}Cl nuclei with the magnetic field along the line between neighbor nucleus and silver nucleus is shown in Fig. 7 for the Ag^0 center in NaCl. The three sets of peaks in the experimental data near 39.5, 40.7, and 42.0 MHz are the quadrupole-split lines occurring at about half the hyperfine structure frequency plus the NMR frequency of ^{35}Cl. The lines at half the hyperfine structure frequency minus the ^{35}Cl NMR frequency are not intense enough to appear above the noise of this expanded scan.

The ENDOR lines in Fig. 7 arise from ^{35}Cl nuclei in two first-shell sites located on opposite sides of the silver nucleus. If one site is occupied by a ^{35}Cl ion and the other by a ^{37}Cl ion, the sites are nonequivalent and a single-neighbor spin Hamiltonian provides an adequate description of the ^{35}Cl line positions. Since the natural abundance of ^{35}Cl is about $\frac{3}{4}$, this occurs about $2(\frac{3}{4})(\frac{1}{4}) = \frac{6}{16}$ of the time. If both sites are occupied by ^{35}Cl ions, the sites are magnetically equivalent and a degeneracy arises. A similar problem, the F-center electron interaction with two equivalent neighbor nuclei, has been solved by Feuchtwang,[12] who used a perturbation theory approach and employed symmetric and antisymmetric combinations of product spin functions. The problem is solved in the present

TABLE III. Spin Hamiltonian parameters for the Ag^0 center in NaCl.

Shell	Nucleus	A/h (MHz)	b/h (MHz)	q/h (MHz)
1	^{35}Cl	69.23 ± 0.10	5.01 ± 0.06	$+0.52 \pm 0.04$
2	^{23}Na	3.52 ± 0.03	$b_1 = 0.35 \pm 0.07$ $b_2 = 0.32 \pm 0.10$	$q = 0.10 \pm 0.02$ $\eta = 1.7 \pm 0.4$
3	^{35}Cl	2.23 ± 0.02	0.158 ± 0.014	0.038 ± 0.011
4	^{23}Na	8.74 ± 0.05	0.48 ± 0.03	0.43 ± 0.02

work by diagonalization of the spin Hamiltonian of Eq. (2) with α summed over two neighbor nuclei. The eigenvalues and eigenvectors of the matrix are calculated by computer, followed by calculation of relative transition probabilities for ENDOR transitions.

The vertical dotted lines in Fig. 7 denote positions and relative intensities of ENDOR transitions computed when one ^{35}Cl and one ^{37}Cl neighbor are included in the two-neighbor spin Hamiltonian. The six positions for ^{35}Cl ENDOR lines are the same as predicted by the single-neighbor spin Hamiltonian described earlier. The six ^{37}Cl ENDOR lines occur at lower frequencies than those included in Fig. 7 and are not shown. The electron Zeeman perturbation term produces the predominant contribution to the transition probability because of wave-function mixing caused by off-diagonal $A^\alpha \vec{I}^\alpha \cdot \vec{S}$ and $\vec{I}^\alpha \cdot \vec{B}^\alpha \cdot \vec{S}$ terms.

The vertical solid lines in Fig. 7 show the positions predicted by the two-neighbor spin Hamiltonian for two ^{35}Cl nuclei. The computer-determined nuclear-spin eigenfunctions are analogous to those determined by Feuchtwang, as are the quantum-number assignments of the states. The relative transition probabilities for the degenerate and nondegenerate cases are compensated by the ratio of occurrence of the two cases. The results give fairly good agreement for most line positions and relative intensities for the three-highest frequency lines.

It is interesting to note that the nondegenerate lines appear to have broader linewidths than the most intense degenerate lines. It is postulated than random strains in the crystal might account for this behavior. Such random strains introduce small changes in the hfs constants by causing shifts of the silver atom relative to its first shell neighbors. It is determined by trial and error that a change in A/h of 0.1 MHz or a change in b/h of 0.2 MHz is necessary to cause a shift of a nondegenerate peak by half its line width at half amplitude. Then this change is applied to the degenerate case by increasing A or b for one neighbor and decreasing A or b for the other neighbor by the same amount. The results of this study are shown in Fig. 7 as the horizontal or slanted lines terminated by dots. The dots show the new line positions and intensities when the above changes are made. Some of the less intense degenerate lines show considerable movement, whereas the most intense degenerate lines show little motion. Thus the random strain hypothesis does offer a reasonable explanation of the differing linewidth for the major degenerate and nondegenerate lines.

Second-order hyperfine structure is also observed and has been analyzed for pairs of shell-4 ^{23}Na nuclei for the Ag^0 center in NaCl and for pairs of shell-1 ^{35}Cl nuclei for the Ag^0 center in KCl. No new features were discovered in these cases.

IV. DISCUSSION OF RESULTS

A. Reconstruction of ESR superhyperfine structure

The ENDOR parameters of Tables I and II can be used to reconstruct the ESR shf structure of the Ag^0 center in KCl and NaCl. The contributions of shells 1, 2, and 4 are taken into account discretely by developing a line spectrum by computer. To take into account the influence of shell 3, each discrete line is then replaced by a Gaussian,[9,13] whose width is determined by shell-3 contributions.

Comparisons with experiment of the fabricated first-derivative ESR spectra of the Ag^0 center in KCl and NaCl are shown in Fig. 8. The ESR spectrum of KCl is fit well with four shells of ENDOR data. The NaCl case shows that the first four ENDOR shells do not produce all of the broadening of superhyperfine lines that is observed experimentally, but it is seen that these shells are major contributors to this broadening. Apparently there still are significant contributions from outer shells, probably from shell-5 chlorine nuclei. Unidentified ENDOR lines were seen near the frequency of shell-3 ^{37}Cl ENDOR lines in NaCl but were not studied in detail in the present work.

B. Ag^0 5*s* electron envelope function

With the use of Gourary-Adrian amplification factors[14] the probability density of the extra electron at a neighbor lattice site can be calculated from the experimentally determined Fermi contact interactions, and the results are shown by the solid dots in Fig. 9 for the Ag^0 center in KCl and NaCl. Also shown are Herman-Skillman[15] theoretical atomic 5*s* envelope functions and experimental and theoretical *F*-center envelope functions.

Some qualitative statements can be made comparing the envelope functions of the extra electron at a free silver atom, a Ag^0 center, and an *F* center. First of all, the potential experienced by a 5*s* electron in an isolated silver atom is a deep attractive potential well inside the shielding effects of the core electrons and an attractive $1/r$ potential far outside the core electrons. When the silver atom is placed in a substitutional cation site in the crystal, the atomic potential is augmented by a repulsive crystal potential, essentially a square well inside the nearest-neighbor shell, plus a positive $1/r$ potential outside. Hence the potential is raised for all regions of the 5*s* electron in the crystal. Under these circumstances

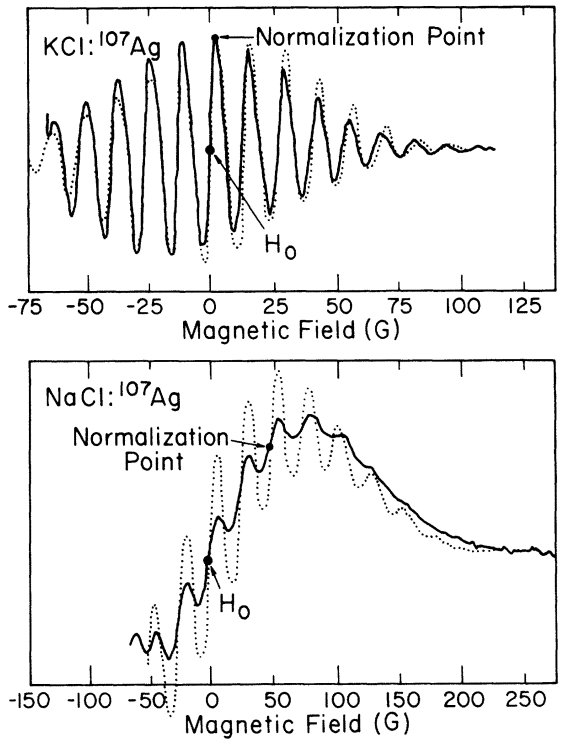

FIG. 8. Comparison of first derivatives of experimental and theoretical shf structure of the high-field ESR line for the Ag^0 center in KCl:^{107}Ag and NaCl:^{107}Ag. The solid lines represent the experimental data. The theoretical curves are represented by the dotted lines. The theoretical curves were normalized to the experimental curves at the indicated points.

we might expect the Ag^0 electron to have a smaller binding energy and to spread out more at the near shells than would be indicated by the atomic envelope function. This is seen somewhat in our results through the first three shells, although the use of amplification factors yields only a qualitative comparison. However, the behavior at shell 4 is definitely anomalous in both crystals. A possible explanation for the anomaly is given at the end of this section.

For an electron at an F center the potential is exclusively an attractive crystal potential since there is no atomic core. Inside the first shell, the potential well is still deeper for the Ag^0 center, but outside this region the attractive $1/r$ tail for the F center is stronger because the Ag^0 electron sees a neutral lattice. These are conflicting influences; apparently the deeper well inside is more important since Fig. 9 shows that the F electron is more spread out.

The shell-4 hyperfine interaction constants for Ag^0 centers in both KCl and NaCl exceed those of shell 2 in their respective crystals. A possible explanation for the large shell-4 contact interactions is a transfer of spin density by a shell-1 Cl^- ion through a $3p_x$ orbital. Wood[19] has noted that this effect occurs in the F center through the (0, 0, 2) Cl^- ion to the (0, 0, 3) K^+ ion and helps explain the larger-than-expected shell-9 Fermi contact interaction. This effect is not present for shell 2 since the Cl^- $3p_x$ or $3p_y$ orbitals, which have an appreciable overlap with the shell-2 cation, have zero overlap with the Ag^0 electron because of symmetry. The results in Fig. 9 are in accord with the highly directional aspect of this proposed mechanism.

C. Electric field gradients and lattice distortion

The quadrupole interaction constants from Tables II and III are plotted as electric field gradients (efg) in Fig. 10. Appropriate Sternheimer antishielding factors, as given in the figure legend, have been used in the expression $(1-\gamma_\infty)$ involved in the conversion. A dimensionless plot is obtained by expressing the shell radius in units of the anion-cation distance d and the efg in units of e/d^3. One striking feature of the figure is the remarkable similarity of the results for the two crystals when plotted in this general form. Additional features are the almost complete cancellation of the point charge efg at shell 3 and the very large observed values of the efg at shell 4.

The significant contributions to the efg at a particular site from nearby point charges have been treated by Feuchtwang[22] and Dick,[23] among others.

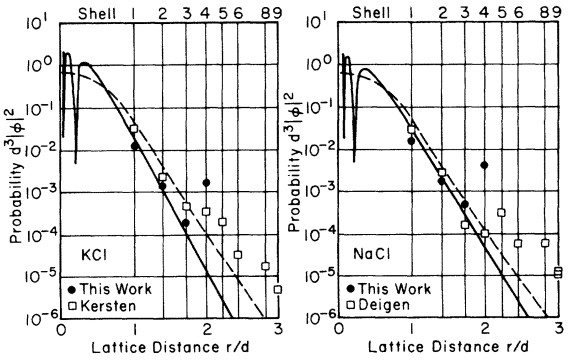

FIG. 9. Theoretical and experimental Ag^0- and F-center wave functions. The solid lines represent the Herman-Skillman (Ref. 15) theoretical envelope function for the 5s electron in a free silver atom. The dashed lines represent the Gourary-Adrain (Ref. 16) Type III theoretical F-center envelope function. The solid circles represent the experimental Ag^0 5s electron probability at neighbor nuclei. The open squares represent the experimental F-center electron probability at neighbor nuclei, computed from experimental measurements of Kersten (Ref. 17) and Deigen *et al.* (Ref. 18). Experimental calculations were performed with the use of the following Gourary-Adrian amplification factors (Ref. 14): 1500 for Cl^-, 650 for K^+, and 260 for Na^+.

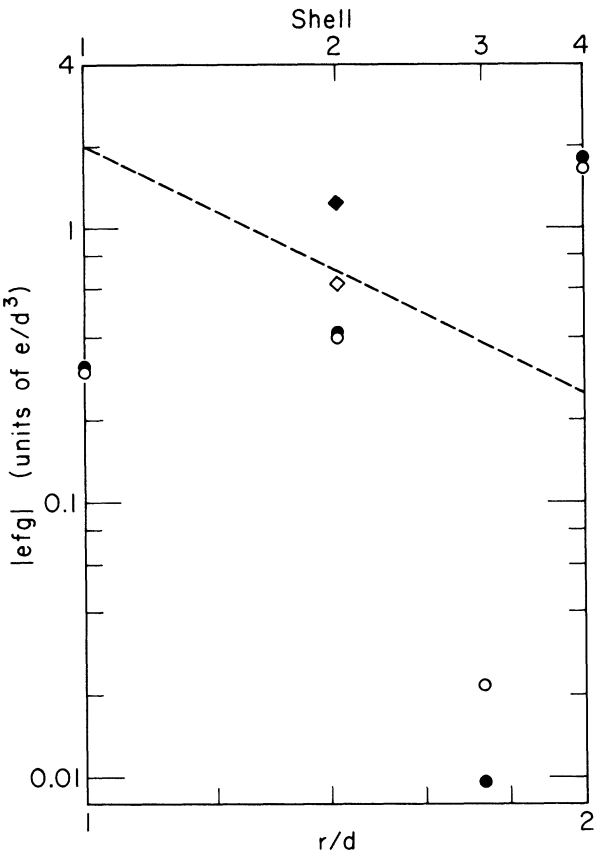

FIG. 10. Absolute magnitude of electric field gradients for Ag^0 centers. Experimental values: ○ and ◇ NaCl, ● and ◆ for KCl; circles show axial values from q, diamonds show nonaxial values from $q' = \eta q$. These are calculated from the observed quadrupole interactions q and q' with quadrupole moments (Ref. 20) of ^{23}Na 0.14, ^{39}K 0.055, ^{35}Cl −0.079 b and Sternheimer factors γ_∞ (Ref. 21) of Na −3.7, K −12, Cl −56. Theoretical values—axial efg of $2r^{-3}$ from an extra point charge at the origin.

(i) The extra electron at the Ag^0 ion, if treated as a point charge at the origin, gives an axial efg of $-2r^{-3}$ in the units used here; this contribution appears as a straight line in the log-log plot of Fig. 10. (ii) The displacement of an ion from its lattice site gives an efg from the Madelung potential that is quadratic in the displacement.[22] (iii) The displacement of the ions in one shell gives an efg at ions of a nearby shell, with both linear[23] and quadratic,[22] and cross terms[22] in the displacements.

Some preliminary comments about lattice distortions in the vicinity of the Ag^0 center can be made by considering qualitatively the influence of these effects. On the basis of ionic radii—Na^+ 0.95, K^+ 1.33, Cl^- 1.81 Å; and Ag^+ 1.26, Ag^0 (from metallic silver) 1.44 Å—it appears that displacements will be *outward* and perhaps *large* (possibly even up to 10%–20%). We treat only radial displacements for the first four shells (as required by symmetry), and consider primarily the contributions of the point charge and Madelung potentials to the efg for these preliminary considerations.

The sign of the quadrupole interaction contant q for a chlorine ion in shell 1 can be determined experimentally and agrees with the predicted sign of the efg from a negative charge at the origin, but the observed values are much smaller than the prediction. The discrepancy could reasonably be removed by using values of $\gamma(r) < \gamma_\infty$ for the portion of the Ag^0 electron charge inside the chlorine ion core[24] (a rough estimate gives a correction up to 100%) and by including the Madelung efg for a [100] displacement (the sign of this term is opposite to the efg from the Ag^0 electron).

The experimentally observed axial efg for shell 2 is in rough agreement with the effect expected from a point charge at the origin, but a point charge would not give any nonaxial efg. A cation displacement of 10% along [110] leads to a Madelung efg that cancels most of the discrepancy for the axial efg and also contributes a nonaxial efg of just about the observed amount.

A displacement of shell-3 anions along [111] causes a Madelung efg of the *same* sign as that from the Ag^0 electron and therefore *cannot* account for the almost complete cancellation in the observed quadrupole interactions. This leaves only displacements of ions in other shells as a possible means of explaining the cancellation. The fact that the cancellation is nearly complete in *both* crystals remains surprising.

For shell-4 ions a displacement of almost 20% would be needed for the Madelung efg to account for the very large observed values. A smaller displacement at shell 4 (perhaps more like 10%) appears likely, with additional contributions to the efg from displacements of other shells.

These qualitative observations suggest that there must be fairly large outward displacements (of the order of 10%) of shells 1 and 4 along [100], somewhat smaller but still appreciable outward displacements of shells 2 and probably 5, and almost no displacement of shell 3. Kersten's calculated *a priori* displacements around the F center in KCl show the same pattern but much smaller values (1%, 0.25%, −0.025%, and 0.28% for shells 1 to 4, respectively).[25] Halliburton *et al.*[26] have observed a similarly small quadrupole interaction at shell 3 for the F^+ center in MgO, and they also find comparable displacements (about 7% and −3% for shells 1 and 4). A more thorough

treatment of the quadrupole interaction for the Ag^0 center is in progress.

ACKNOWLEDGMENTS

We wish to express our thanks to the Physics Department at Ohio University, Athens, for the temporary loan of some of the equipment used in this investigation, and to the Radiation Biophysics Department at the University of Kansas, for the use of their γ-ray source. We also wish to thank Professor J. W. Culvahouse for stimulating discussions regarding this work. Computer calculations were performed at the University of Kansas Computation Center.

---

†This paper is based on a dissertation presented by one of the authors (G.E.H.) to the Graduate School, University of Kansas, in partial fullment of the requirements for the degree of Doctor of Philosophy in Physics.

*NASA Trainee 1968–1970 and 1971–1972.

‡Present address: Dept. of Physics and Astronomy, University of North Carolina, Chapel Hill, N. C. 27514.

[1]C. J. Delbecq, W. Hayes, M. C. M. O'Brien, and P. W. Yuster, Proc. R. Soc. Lond. A 271, 243 (1963).

[2]H. Seidel, Phys. Lett. 6, 150 (1963).

[3]P. G. Baranov, R. A. Zhitnikov, and N. I. Melnikov, Phys. Status Solidi 30, 851 (1968).

[4]P. G. Baranov, R. A. Zhitnikov, and N. I. Melnikov, Phys. Status Solidi 30, 859 (1968).

[5]P. G. Baranov, R. A. Zhitnikov, and N. I. Melnikov, Phys. Status Solidi 33, 463 (1969).

[6]N. I. Melnikov, R. A. Zhitnikov, and P. G. Baranov, Fiz. Tverd. Tela 13, 1337 (1971) [Sov. Phys.-Solid State 13, 1117 (1971)].

[7]W. P. Unruh, L. G. Nelson, J. T. Lewis, and J. L. Kolopus, J. Phys. C 4, 2992 (1971).

[8]G. Breit and I. I. Rabi, Phys. Rev. 38, 2082 (1931).

[9]G. E. Holmberg, Ph.D. thesis (University of Kansas, 1972) (unpublished).

[10]*Nuclear Magnetic Resonance Table*, 5th ed. (Varian Associates, Palo Alto).

[11]G. Wessel and H. Lew, Phys. Rev. 92, 641 (1953).

[12]T. E. Feuchtwang, Phys. Rev. 126, 1628 (1962).

[13]J. H. Van Vleck, Phys. Rev. 74, 1168 (1948).

[14]H. Seidel and H. C. Wolf, in *Physics of Color Centers*, edited by W. B. Fowler (Academic, New York, 1962).

[15]F. Herman and S. Skillman, *Atomic Structure Calculations* (Prentice-Hall, Englewood Cliffs, N. J., 1963).

[16]B. S. Gourary and F. J. Adrian, in *Solid State Physics*, edited by F. Seitz and D. Turnbull (Academic, New York, 1960), Vol. X, p. 127.

[17]R. Kersten, Phys. Status Solidi 29, 575 (1968).

[18]M. F. Deigen, V. Ya. Zevin, S. S. Ischenko, N. P. Baran, M. A. Rubin, and V. V. Teslenko, Phys. Status Solidi 37, 237 (1970).

[19]R. F. Wood, Phys. Status Solidi 42, 849 (1970).

[20]G. H. Fuller and V. W. Cohen, Nuclear Data Tables A 5, 433 (1969).

[21]E. A. C. Lucken, *Nuclear Quadrupole Coupling Constants* (Academic, New York, 1969).

[22]T. E. Feuchtwang, Phys. Rev. 126, 1616 (1962).

[23]B. G. Dick, Phys. Rev. 145, 609 (1966); T. P. Das and B. G. Dick, *ibid.* 127, 1063 (1962).

[24]H. M. Foley, R. M. Sternheimer, and D. Tycko, Phys. Rev. 93, 734 (1954).

[25]R. Kersten, Ph.D. thesis (University of Stuttgart, 1970) (unpublished).

[26]L. E. Halliburton, D. L. Cowan, and L. V. Holroyd, Solid State Commun. 12, 393 (1973).